A region-based cross-correlation approach for tonometric carotid–femoral Pulse Wave Velocity Assessment

Biomedical Signal Processing and Control 93 (2024) 106161

Contents lists available at ScienceDirect

Biomedical Signal Processing and Control

journal homepage: www.elsevier.com/locate/bspc

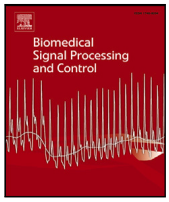

A region-based cross-correlation approach for tonometric carotid–femoral Pulse Wave Velocity Assessment

Andrea Valerio [a,*], Irene Buraioli [a], Alessandro Sanginario [a], Giulia Mingrone [b], Dario Leone [b], Alberto Milan [b], Danilo Demarchi [a]

[a] Department of Electronics and Telecommunications, Politecnico di Torino, Torino, 10129, Italy
[b] Department of Medical Sciences, Internal Medicine and Hypertension Division, University of Torino - AOU Città della Salute e della Scienza di Torino, Torino, 10126, Italy

ARTICLE INFO

Keywords:
Pulse Wave Velocity
cfPWV
Pulse transit time
Arterial stiffness
Cross-correlation
Blood pulse

ABSTRACT

This work introduces a novel region-based algorithm to determine carotid–femoral Pulse Wave Velocity (cfPWV), decoupling the assessment of this biomarker from point-to-point feature extraction. A dataset of 75 healthy participants, previously recruited to compare the performances of a new instrument, Athos, with the gold standard for non-invasive PWV (SphygmoCor), was used to set up a new algorithm for determining the clinical cfPWV. The proposed approach locates and processes a specific window on the carotid and femoral signals. Cross-correlation is employed to compute the pulse transit time within the pulses. Finally, the cfPWV is assessed. A set of indicators has been defined to quantify the stability and reliability of the window used by the algorithm. The results obtained through the proposed algorithm, the Intersecting Tangent method, and the direct application of the cross-correlation technique on signal epochs have been systematically compared with outcomes derived from the SphygmoCor device. The retrieved results show a Pearson coefficient $r = 0.96$, $P < 0.001$, with a mean difference of $0.16\,m/s$ for the first case, $r = 0.965$, $P < 0.001$, with a mean difference of $-0.07\,m/s$ for the second, and $r = 0.82$, $P < 0.001$, with a mean difference of $-1.04\,m/s$ for the third. Despite the intersecting tangent method showing slightly better agreement when comparing cfPWV values with those derived from the SphygmoCor, the proposed approach yields significantly lower errors ($P < 0.05$) in the presence of different levels of added noise, demonstrating greater robustness in this context. This outcome, combined with the excellent accuracy, sustains the suitability of the proposed method for clinical applications.

1. Introduction

Vascular aging has been demonstrated to be linked with an increment in the chance of developing chronic illnesses such as cardiovascular disease (CVD), type 2 diabetes and renal disorder [1–3]. Among the non-invasively possibilities, the Pulse Wave Velocity (PWV) measurement is the most reliable. PWV is the transit velocity of blood pulse waves through the arterial system [4]. It depends on the vascular biomechanics and hemodynamics of the circulatory system [5,6]. It provides information about compliance [7], mean arterial pressure [8], vasomotor tone [7] and therapeutic efficacy in vascular and hypertensive heart diseases [9–12]. In 2007, it was officially introduced in the European Society of Cardiology and Hypertension guidelines as a valuable predictor of cardiovascular risk stratification and an effective tool for detecting asymptomatic organ damage [13,14].

According to Eq. (1), PWV is computed as the ratio of the distance between two sites d and the time required by the blood pulse to circulate from one site to the other Δt.

$$PWV = \frac{d}{\Delta t} \tag{1}$$

PWV can be measured between any two sites in the circulatory system. However, the two acquisition points determine whether the parameter obtained is local or global [4]. Due to the proximity of the two acquisition sites to the central aorta, carotid–femoral pulse wave velocity (cfPWV) is recognized as the most widely measured surrogate of the aortic-pulse wave velocity (aPWV) [15–17]. With the introduction of PWV as a standard biomarker of arterial stiffness, several methodologies and algorithms have been developed to provide increasingly accurate estimates of PTT. As a result of the analysis of the

Abbreviations: PWV, pulse wave velocity; PTT, pulse transit time; RBCC, region-based cross-correlation; CV, coefficient of variation; intraSV, intra subject variability; interSV, inter subject variability

* Corresponding author.
E-mail address: andrea.valerio@polito.it (A. Valerio).

https://doi.org/10.1016/j.bspc.2024.106161
Received 16 August 2023; Received in revised form 13 February 2024; Accepted 24 February 2024
Available online 28 February 2024

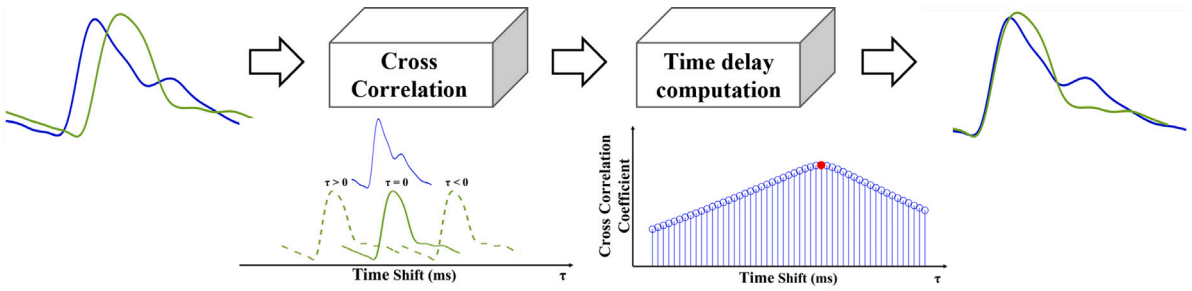

Fig. 1. Pulse waveforms alignment performed using cross-correlation. Given the carotid pulse (blue) and the femoral pulse (green), the cross-correlation function is computed for each value of τ. The timeshift's equivalent which leads to the maximum of the cross-correlation function is taken as pulse transit time, then the alignment is performed.

characteristic morphology of the pulse wave [18], numerous studies over the years have proposed the identification of a specific point or window on the signal that would allow reliable PWV estimation [17]. Different algorithms relying on the extraction of a single feature located on the signal were used for PTT assessment. Among these, the most employed technique is the *foot* of the upstroke of the blood pulse as a reference point in the waveform [19]. However, as reported in [20–22], these approaches, when applied to identical waveforms, might result in differing PWV values. Nowadays, many clinical indicators, including heart rate and blood pressure, may now be monitored by wearable devices with findings that meet the standards for use in a clinical setting. Many studies have been conducted to assess PWV using standalone wearable devices, following this trend. The extraction of pulse waves from acquisition locations that deviate from clinically defined places may alter the shape of the signals, hence diminishing the estimated precision of the techniques described above. A novel set of algorithms has been developed to address the limitations of relying on a single localized feature for PWV evaluation. These algorithms analyze specific sections of pulse waveforms, avoiding the PWV evaluation based on a single feature extracted from the signal. Although additional validation studies must be undertaken, region-based approaches such as 'diastole patching' [19] and 'region-matching' [17,23] provided excellent accuracy in the PWV assessment according to the accuracy criteria reported in 2010 ARTERY Society guidelines [24]. In this manuscript, we present a novel region-based algorithm for the estimation of cf-PWV. Specifically, our method applies several processing steps to the waveform recorded on both sites, then, it uses the cross-correlation technique to assess the PTT. Given two generic time series $X_c(t)$ and $X_f(t)$, both defined in the time interval T, the cross-correlation is a statistical technique used to quantify their delay along the abscissa according to the continuous time shift τ. It is defined as expressed in Eq. (2).

$$R_{X_c,X_f}(\tau) = \frac{1}{T}\int_{-\frac{T}{2}}^{\frac{T}{2}} X_c(t)X_f(t+\tau)dt \tag{2}$$

In this case, the two time series to be compared are the pulse waveforms detected on the carotid and femoral sites, respectively defined as X_c and X_f. T represents a fraction of the full cardiac cycle and τ constitutes the time shift along the abscissa by which the cross-correlation coefficient is computed. The cross-correlation function, $R_{X_c,X_f}(\tau)$, is estimated for each value of τ. When the maximum of $R_{X_c,X_f}(\tau)$ occurs, the best achievable similarity condition is reached and τ is considered as the PTT. Fig. 1 shows an example of the realignment of two pulse waveforms using cross-correlation. As mentioned in [4,25,26], cross-correlation was previously used to calculate the PTT. However, its application was employed only in a local assessment of the PWV. This limitation was mainly due to morphological differences presented by the pulse waves at the two distant acquisition sites. The proposed approach aims to overcome this issue by giving as input for the cross-correlation a set of signals characterized by a known shape in which the portion of signal used for the PTT calculation remains unchanged along the sites. Results equivalent to those obtained from the reference device were achieved, representing a significant improvement over the direct application of cross-correlation to the original signals. This article is structured as follows. Section 2 introduces the available data, the proposed algorithm, the methodology employed to identify the processing window and the carried out statistical analysis. Section 3 summarizes the results obtained by the Region-Based Cross-Correlation (RBCC) approach compared to the direct application of cross-correlation technique and the output of the two presented devices. The reported results are discussed in Section 4. Finally, in Section 5, conclusions are presented.

2. Material and methods

2.1. Experimental data

Two devices for PWV analysis were used to collect the pulse waveforms obtained in this study: the Athos system, whose hardware and firmware conceptualization and development are detailed in [13], and the SphygmoCor (AtCor Medical). The former was used to retrieve the blood pulse raw data, while the latter was used as the reference method to compare the achieved outcomes. The SphygmoCor is widely regarded as the clinical gold-standard device used for the non-invasive cfPWV assessment [14,24]. Both devices determine the PWV value by locating the intersecting tangent (IT) method recognized as the most reliable among the single-feature algorithms introduced in the previous section. The data used for developing the algorithm were acquired at the "Città Della Salute e Della Scienza" hospital in Turin (Italy) according to the experimental protocol approved by the "University of Turin Bioethical Committee". A cohort of 75 healthy subjects was recruited to validate the precision and accuracy of the Athos device [27]. In this particular context, the device was analyzed from a clinical perspective, emphasizing its application, intraoperator variability, and estimation accuracy. As a result of the mentioned study, we employed Athos for three main reasons: an excellent level of agreement with the Sphygmocor, high quality of pulse waveforms, and finally, differently from the reference device, it provides access to the raw data. The pulse waveforms collected in the mentioned study were recorded with a sampling frequency of 680 Hz and subsequently stored for offline processing in the Matlab environment.

2.2. Proposed algorithm

The main steps of the herein-reported RBCC algorithm are summarized in Fig. 2. In particular, this can be divided into three main phases: *pre-processing*, *processing* and *evaluation of the outcome*. The pre-processing phase is characterized by a series of filter steps used to remove the DC-bias and high-frequency noise and to retrieve the cardiac activity of the subject under investigation. The delay and the phase distortion introduced by the application of each filter were removed by applying this latter forward and backward onto the signal. Fig. 3 reports the steps used for extrapolating the cfPWV of the acquired signals.

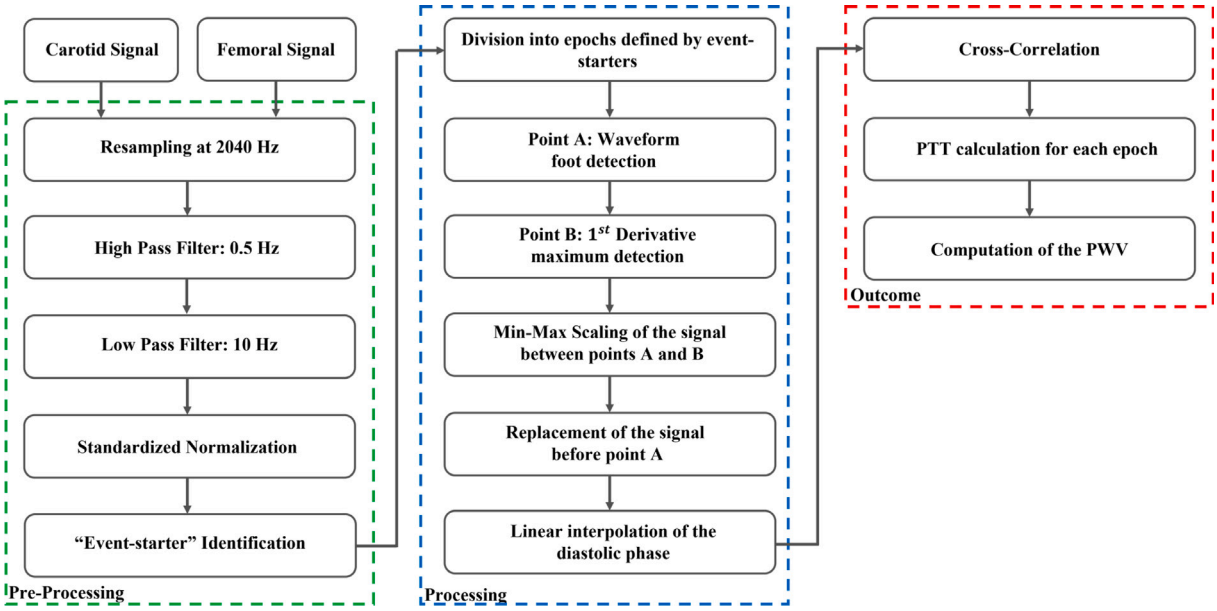

Fig. 2. Illustration of the presented Region-Based Cross-Correlation (RBCC) algorithm divided into its macro stages: *pre-processing*, *processing* and *evaluation of the outcome*.

(*i*) To get a high time resolution for the assessed PTT, the tonometer signal is resampled to 2040 Hz through a cubic spline. As a result of this resampling, the signal temporal resolution is increased to 0.49 ms. Interpolation is accomplished using a third-degree polynomial with forced continuity in the second derivate.

(*ii*) As reported in [13,26], high pass filter with a cut-off frequency equal to 0.5 Hz is applied to remove the DC offset.

(*iii*) Subsequently, a low pass filter with a cut-off frequency equal to 10 Hz is used to remove the high-frequency noise [26].

(*iv*) Once done with the filter steps, pulse waveforms are standardized [26] according to Eq. (3):

$$x = \frac{x - \mu_s}{\sigma_s} \tag{3}$$

where μ_s and σ_s are respectively the mean value and the standard deviation of the signal. The result of the filtering steps is shown in Fig. 3(a).

(*v*) This step uses the carotid signal to evaluate the subject cardiac periodicity (T), which in turn is employed to split the signals into single epochs. To do so, a low pass filter with a cut-off frequency of 1.5 Hz is applied. The beginning of each cardiac period is detected as the minimum points of the filtered carotid signal, as represented by green asterisks in Fig. 3(b).

(*vi*) The projection of the points, found in the previous step, on the abscissa, is used as the common reference to divide both carotid and femoral signals, Fig. 3(c). In this way, it is possible to process each couple of blood pulses preserving the information concerning the time delay related to the propagation of the pulse wave between the two sites.

(*vii*) The initial step in the processing phase is to find the closest minimum point preceding the upslope of the pulse. This position corresponds to the diastolic minimum, point A in Fig. 3(d). Point O identifies the beginning of each pulse wave.

(*viii*) Point B, depicted in Fig. 3(d), represents the second point used to define the window on the original signal. This characteristic point is located at the maximum point of the first derivative of the signal. Finally, point C identifies the end of the pulse wave.

(*ix*) Once the window is recognized on both pulses, these are normalized [26]. This is to ensure that both waves are on the same baseline and to avoid the different amplitudes of the rising fronts that could affect the cross-correlation result, Fig. 3(e, f).

(*x*) To preserve the time delay between the two waves, the portion of the pulse between points O and A is replaced by a number of samples equal to the number of samples on the original signal. Concerning the portion of the signal between points B and C, this section is linearly interpolated on the same number of samples which separates B and C on the abscissa.

(*xi*) The time delay at which the maximum of cross-correlation coefficient occurs indicates the time shift that gives the best alignment, Fig. 3(g,h).

(*xii*) Once the PTT value for the current epoch is found, the process starts again from step *(vii)*. The procedure continues until the PTT values for all N epochs, segmented at *(vii)*, are obtained.

(*xiii*) The standard deviation (σ) is calculated for the retrieved data. To enhance comparison with the Sphygmocor device, we adopted the same outlier rejection criteria. Hence, PWV values outside the range of $\pm 0.9\sigma$ are rejected.

(*xiv*) Finally, the remaining PWV values, E, are computed and averaged as reported in Eq. (4).

$$\bar{PWV} = \frac{1}{E}\sum_{j=1}^{E}\frac{d}{PTT_{car-fem}(j)} \tag{4}$$

Where d represents the distance measured between the femoral and the carotid acquisition sites multiplied by a correction factor equal to 0.8 [4,28]. This correction factor accounts for the overestimation of the aortic length calculated on the subject's skin.

2.3. Robustness of the algorithm

The term algorithm robustness refers to the algorithm's capacity to perform the cfPWV assessment despite interference conditions caused by the presence of noise or artifacts superimposed on the signal. Within the context of this application, a white Gaussian noise was introduced onto the pulse wave signals in order to obtain signal-to-noise ratios (SNRs) of 10, 15, 20, and 25 dB across the bandwidth of the signal (i.e., 0.5–10 Hz) [25]. Each measured pulse wave signal was denoised through the application of filtering stages reported in the processing steps *(ii)* and *(iii)* of the proposed algorithm. Subsequently, the resultant signal served as the starting point for the addition of noise needed to achieve the specified SNRs. Then, both algorithms, RBCC and ITP, were applied to the noisy pulse wave signals. Finally, we compared

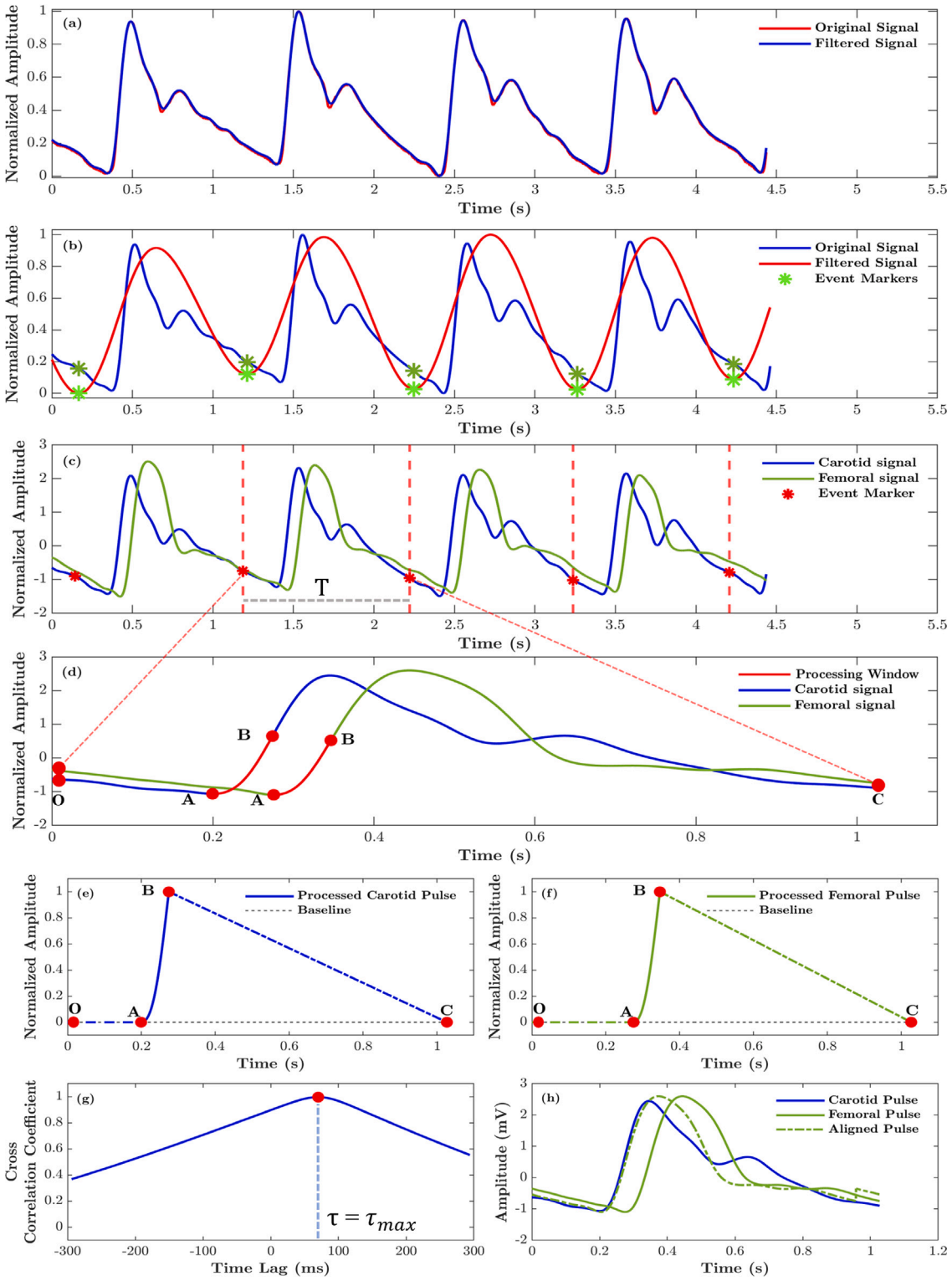

Fig. 3. Region Based Cross-Correlation (RBCC) algorithm processing steps. **(a)** Result of the bandpass filtering procedure: original signal (blue), filtered signal (red). **(b)** Individuation of the cardiac activity (green points) on the low pass filtered carotid signal (red). **(c)** Carotid signal (blue) and femoral signal (green) are split into single epochs. **(d)** Detection of the processed windows on both signals in the current epoch. **(e)** Processed carotid window. **(f)** Processed femoral window. **(g)** Evaluation of the delay through the application of the cross-correlation technique on the mentioned windows. **(h)** Alignment of the processed signals in the current epoch.

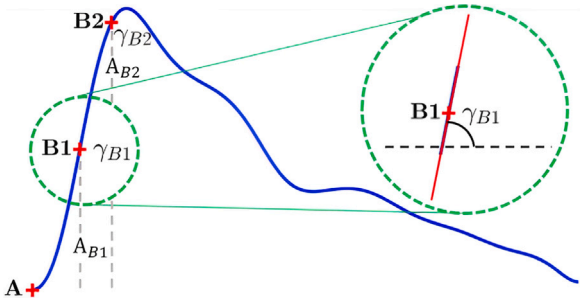

Fig. 4. Selected points used for the definition of the processing window. End of the diastole (A), the maximum of the first derivative (B1) and the 95% of the systolic peak amplitude (B2). The slope coefficient γ has been computed as the angle between the horizontal line and the tangent line passing through successive samples on the signal. The value assumed by γ in B1 and B2 was defined as γ_{B1} and γ_{B2}.

the resulting differences between noisy-cfPWV values and those derived from the application of each method on noise-free signals.

2.4. Identification of processing window

Since the proposed algorithm relies on the application of the cross-correlation on a specific portion of the signal, it is necessary to point out how the processing window was defined. As stated in [29], pulse waveforms acquired from different places on the human body have distinct morphologies. Particularly, the shape of blood pulses may be altered by several factors, including the positioning of sensors on the skin, the experience of the operator collecting the data and the subject's anatomy. The decision to define a specific section of the signal derives from the necessity of minimizing the morphological disparities between individual pulse waves while preserving the temporal information. As reported in [19,30–32], the early systolic and end-diastolic portions of the blood pulse are identified as the least likely to be impacted by reflected waves and motion artifacts compared to the diastolic component. Therefore, the search for processing window was made by analyzing the amplitude and the slope of the rising front of all the waveforms available in the dataset. The inclination of the curve was derived by computing the point-by-point slope γ of the tangent line with respect to the horizontal. The tangent to the curve was determined using the known equation of the line passing between two points for each pair of successive samples. The slope γ has been computed according to Eq. (5).

$$\gamma = \arctan\left(\frac{df(t)}{dt}\right) \tag{5}$$

Where $f(t)$ represents the pulse waveform as a function of time t. Fig. 4 illustrates the points considered for defining the processing window. The minimum preceding the ascending portion of the systolic phase, indicated as A, represents the window's lower boundary. Concerning the definition of the upper limit, two specific points have been considered. The first one corresponds with the maximum of $\gamma(t)$, (B1), and the one located at 95% of the systolic peak's amplitude (B2). This latter option was preferred to the systolic peak since the calculated slope at the signal's maximum would always be zero, as the tangent line becomes horizontal whenever a local, or global, minimum, or maxima occurs.

2.5. Statistical analysis

The following subsection describes the statistical analysis used to determine the upper bound of the window as well as the parameters employed to evaluate the algorithm's performance for estimating from the PWV. Three different indicators have been defined to quantify the stability of the mentioned upper boundary across the entire dataset: the intra-subject variability *(intraSV)*, the inter-subject variability *(interSV)* and the coefficient of variation *(CV)*. The *(intraSV)* evaluates the overall point-to-point difference of the considered features in B1 and B2 on the carotid and femoral sites. This information enabled us to determine which of the two points leads to the section of the signal presenting the highest similarity, hence improving the algorithm's precision. As reported in Eq. (6), the first step in the calculation of this parameter is to determine the absolute difference, D_i, of the considered feature for each couple of carotid and femoral waves.

$$D_i = \left| feat_{CAR,i} - feat_{FEM,i} \right| \qquad feat = A, \gamma. \tag{6}$$

Where A, refers to the amplitude value and γ to the slope coefficient assumed in B1 or B2. Subsequently, the average difference $\overline{D}_k$ was computed for each subject k, Eq. (7).

$$\overline{D}_k = \frac{1}{n_k}\sum_{i=1}^{n_k} D_i \tag{7}$$

Where n_k is the number of pulses available for the *k-th* subject. Once obtained a representative value for each subject, they have been further averaged according to Eq. (8)

$$\overline{\mu}_D = \frac{1}{M}\sum_{i=1}^{M} \overline{D}_k \tag{8}$$

M represents the number of subjects in the dataset. Then the standard deviation $\overline{\sigma}_D$ has been computed according to Eq. (9)

$$\overline{\sigma}_D = \sqrt{\frac{1}{M}\sum_{i=1}^{M}(D_i - \overline{\mu}_D)^2} \tag{9}$$

Combining Eqs. (8) and (9) the intra subject variability *(intraSV)* is finally retrieved, Eq. (10)

$$intraSV = \overline{\mu}_D \pm \overline{\sigma}_D \tag{10}$$

The second parameter defined for this purpose is inter-subject variability *(interSV)*. This indicator assesses the variability of the values assumed by the amplitude and the slope in B1 and B2. It provides information on the variation of the features, in the mentioned points, on the carotid and femoral signals. The first executed step in the calculation of this parameter is the mean value $feat_k$ defined in Eq. (11)

$$\overline{feat}_k = \frac{1}{n_k}\sum_{i=1}^{n_k} feat_i \qquad feat = A, \gamma. \tag{11}$$

Where n_k is the number of pulses available for the *k-th* subject. The standard deviation σ_k for the *k-th* subject is computed according to Eq. (12)

$$\sigma_k = \sqrt{\frac{1}{n_k}\sum_{i=1}^{n_k}(feat_i - \overline{feat}_k)^2} \tag{12}$$

Similar to what was conducted with *intraSV*, the results obtained for each subject using Eqs. (11) and (12) were combined to calculate representative values for the entire dataset using Eqs. (13) and (14).

$$\overline{\mu} = \frac{1}{M}\sum_{i=1}^{M} \overline{\alpha}_k \tag{13}$$

$$\overline{\sigma} = \sqrt{\frac{\sum_{k=1}^{M}(n_k - 1)\sigma_k^2}{\sum_{k=1}^{M}(n_k) - M}} \tag{14}$$

Where M is the number of participants. Inter-subject variability *(interSV)*, defined as Eq. (15), is reported below

$$interSV = \overline{\mu} \pm \overline{\sigma} \tag{15}$$

The coefficient of variation *(CV)* defined in Eq. (16), as the ratio between the average standard deviation $\overline{\sigma}$ and the mean value $\overline{\mu}$, has been used to compare the variability of the measurement respect to its

Table 1
Indicators employed in the processing window's upper boundary assessment.

Feature	Indicator	B1		B2	
		CAR	FEM	CAR	FEM
Slope	CV (%)	4.3	5.4	22.9	18.8
	interSV (DEG)	73.10 ± 3.14	71.80 ± 3.88	43.04 ± 9.84	40.2 ± 7.5
	intraSV (DEG)	6.22 ± 3.14		14.87 ± 7.15	
Amplitude	CV (%)	19.9	19.8	20.5	24.8
	interSV (μV)	51.5 ± 10.2	51.8 ± 10.2	110.1 ± 22.5	110.6 ± 27.7
	intraSV (μV)	19.6 ± 12		41.9 ± 25.5	

Abbreviations: CV; coefficient of variation, interSV; inter-subject variability, intraSV; intra subject variability.

mean value, in the mentioned points, using the extracted angles and the amplitude.

$$CV(\%) = \frac{\overline{\sigma}}{\overline{\mu}}.100 \tag{16}$$

Concerning the PWV estimation, each participant was evaluated through 3 acquisitions using the two available devices. The results obtained have been expressed in terms of mean value and standard deviation. The performance of the proposed algorithm has been evaluated by comparing the average PWV values with those obtained with the Athos system, the SphygmoCor, and the simple cross-correlation technique (i.e. applied without carrying out the steps to select the processing window previously described). The Pearson correlation coefficient and the paired t-test analysis have been used to assess the relationship between the available PWV values. Furthermore, a linear regressive model has been used to quantify the concordance of the measurements and its goodness evaluated through the determination coefficient R^2. Measurement accuracy was assessed by calculating the mean value, standard deviation, and root mean square error (RMSE) of the difference between the reference method and the method to be tested. The concordance of the measurements with the reference device was examined employing the Bland–Altman plot, and the significance of the data was evaluated by setting $P < 0.05$. Regarding the application of the proposed algorithm w.r.t the IT, both approaches were applied to the noisy pulse wave signals; the resulting PWV values were compared to those obtained with those derived from the application of IT and RBCC on noise-free signals. Particularly, the absolute error for the *i-th* subject, w.r.t the noise-free cfPWV, was computed as reported in Eq. (17).

$$error\ [i]_{\alpha,\beta} = \left| cfPWV\ [i]_{\alpha,\beta} - cfPWV\ [i]_{\alpha,\ noise\ free} \right| \tag{17}$$

Where $cfPWV\ [i]_{\alpha,\beta}$ refers to the cfPWV value for the *i-th* subject according to tested method ($\alpha \in$ {RBCC, IT}) and β to the related SNR value ($\beta \in \{10\,\text{dB}, 15\,\text{dB}, 20\,\text{dB}, 25\,\text{dB}\}$). Then, the mean absolute error was computed for each SNR for the two algorithms. The multi-sample non-parametric Friedman test [25,33] was employed to assess the statistical significance of the observed errors for IT and RBCC, coupled according to the tested SNRs (e.g. $error_{IT,\,10\,\text{dB}}$ with $error_{RBCC,\,10\,\text{dB}}$ etc.) for a total of four tests. The significance of the identified variations was determined by establishing a threshold at $P < 0.05$.

3. Results

3.1. Processing window assessment

In the prior section, three different indicators have been employed to define the correct feature to identify the best location on signals. The *CV* indicator was used to determine whether to select the slope or the amplitude as the parameter to define the processing window's upper boundary. The *intraSV* was used to quantify the consistency of the tested points within each subject. Finally, *interSV* was employed to assess the stability of those across the entire dataset.

Table 1 reports the CV indicator computed in B1 and B2 for each feature on each acquisition site. For the slope γ, CV is equal to 4.3 % and 5.4 % in B1 and 22.9 % and 18.8 % in B2. Concerning the amplitude value, CV results are equivalent to 19.9 % and 19.8 % in B1 and 20.5 % and 24.8 % in B2.

Table 1 also shows the outcomes of the *intraSV* and *intraSV* used to define the extreme point of the window. For the carotid site, *interSV* results to be equal to $73.10 \pm 3.14°$ in the first point and $43.04 \pm 9.84°$ for the second. For the femoral site, however, *interSV* takes a value of $71.80 \pm 3.88°$ in B1 and $40.2 \pm 7.5°$ in B2. The analysis of the *intraSV* reports an average difference value of $6.22 \pm 3.14°$ for the first case and $14.87 \pm 7.15°$ for the second. Both indicators were utilized to evaluate the stability of the tested points. *IntraSV* specifically examined the variability within data from the same subject, while *inerSV* was computed to observe variations across different subjects.

Table 2
Clinical characteristics of the study population.

Characteristics	Mean ± sd	Range
Number of subjects	75	–
Number of acquisitions	3	–
Number of pulses per acquisition	–	5–14
Total number of pulses	2128	–
Male	43 (57.3%)	–
Age (years)	46 ± 17	19–82
Height (cm)	170.5 ± 10.57	153–195
Weight (Kg)	68.84 ± 14.07	45–106
BMI (Kg m^{-2})	23.56 ± 3.72	17.8–37.11
SBP (mmHg)	117.88 ± 11.53	93–147
DBP (mmHg)	72.89 ± 8	59–94
HR (bpm)	64.44 ± 10.24	41–90

Abbreviations: BMI; body mass index, SBP; systolic blood pressure, DBP; diastolic blood pressure, HR; heart rate, bpm; beats per minute, sd; standard deviation.

3.2. Pulse wave velocity assessment

Table 2 displays the clinical features of the participants who were enrolled in the study. Of the 75 healthy subjects recruited, 43 (57.3%) were men. The average age of the population was 46 ± 17 years, distributed heterogeneously between 19 and 82 years old. The comparison results between the IT method used by the Athos device, the proposed algorithm RBCC, and the direct application of the cross-correlation technique to the signal epochs (DCC) are presented in Table 3. The comparison is performed in relation to the SphygmoCor device. The results obtained show a high correlation between the PWV values obtained in two out of three cases. The Pearson's coefficient retrieved in the three cases is equal to 0.965, 0.96 and 0.82, respectively for IT, RBCC and DCC. The determination coefficient R^2, used to assess how well the regression predictions approximate the real data points, is 0.926, 0.918 and 0.638, revealing the poorer performance of the cross correlation approach when compared to the other methods. The average difference $\pm 2\sigma$ calculated concerning the PWV values estimated by the SphygmoCor and shown in the Bland–Altman plot is -0.07 ± 0.52 m/s for IT, 0.16 ± 0.54 m/s for the RBCC and -1.04 ± 2.21 m/s for the cross-correlation (DCC). The Athos device shows the lowest bias (absolute mean difference) and standard deviation values of the tested methods

Table 3
Accuracy of cfPWV estimated values compared to those extracted by the reference method (SphygmoCor).

Method	Mean difference[a] (m s^{-1})	sd of mean difference	RMSE (m s^{-1})	r	R^2
Intersecting Tangent	−0.07	±0.522	0.519	0.965	0.926
Region Based Cross-Correlation	0.16	±0.544	0.573	0.960	0.918
Direct Cross-Correlation	−1.04	±2.211	2.435	0.820	0.638

Abbreviations: RMSE; root mean square error, r; Pearson's correlation coefficient, R^2; determination coefficient.
[a] Difference of cfPWV estimated values compared to those extracted by the reference device, SphygmoCor.

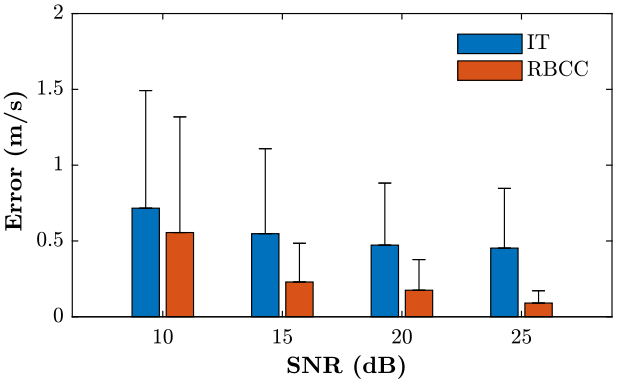

Fig. 5. Mean absolute error and related standard deviation associated to cfPWV values computed at different SNRs with respect to those obtained using Intersecting Tangent (IT) and Region Based Cross Correlation (RBCC) on noise-free signals.

while the cross-correlation technique represents the worst case for all indicators seen so far. A similar condition occurs for the RMSE it is 0.52 for the first method, 0.57 for the second and 2.43 for the third.
Fig. 5 shows the performance of RBCC and IT algorithms when applied on carotid and femoral pulse waveforms corrupted by different levels of noise. The mean absolute error computed w.r.t the PWV values derived from noise-free signals reveals the poor noise tolerance of the IT method despite the tested SNR. Across all four cases, the RBCC algorithm exhibited greater robustness to the introduced noise, demonstrating a lower mean difference along with the associated standard deviation. The statistical analysis, conducted through the Friedman test, consistently yielded $P < 0.05$ in all tested cases when comparing cfPWV absolute differences for each noise level. Three out of four SNRs (15 dB, 20 dB, and 25 dB) reported values largely below 0.01. The only exception lies for the test with an SNR of 10 dB, where the resulting P value remained below 0.05. Nevertheless, despite the increased error and associated standard deviation observed in this instance, all these findings testify the existence of significant differences between cfPWV values derived from the application of IT and RBCC across different noise levels.

4. Discussion

4.1. Processing window assessment

Within this study, a particular focus is given to the methodology used to identify a signal window that enhances the algorithm's performance. The literature suggests that the ascending part of the systolic peak is least affected by motion artifacts and reflection phenomena near vessel branches [19,30–32]. As a result, the minimum point before the systolic peak was chosen as the lower boundary of the processing window. Furthermore, it limited the study of the upper boundary to the aforementioned points B1 and B2. The amplitude and the slope are the features used to characterize points B1 and B2 on every pulse for each of the 75 subjects.

Fig. 6 shows the CV indicator computed in B1 and B2 for each feature on the carotid site (blue) and femoral site (red). Fig. 6(a) shows that the CV takes on values that are equivalent to 4.3% and 5.4% in B1 and 22.9% and 18.8% in B2 when applied to γ. In the second case, Fig. 6(b), CV is equal to 19.9% and 19.8% in B1 and 20.5% and 24.8% in B2 for amplitude values. B1 displays lower CV values than B2, indicating it as the location with less variability. A small value of CV is indicative of greater stability of the identified pulse section over the entire dataset. This is important because although there are intra and inter-subject differences, the chosen portion of the signal maximizes the efficiency of the realignment performed through the proposed approach while preserving the information of interest. In addition, the values of point B1 and point B2 differ more in the bar plot, considering the slope with respect to the one considering the amplitude, where the values are comparable. This mismatch may be due to the pressure produced by the operators during acquisitions, resulting in differing signal amplitude values. Consequently, it can be concluded that γ allows a more precise distinction between B1 and B2 when determining the processing window's upper limit.
Figs. 7(a) and 7(b) depict the computed *intraSV* and *interSV* for the slope γ. Both indicators confirm B1 as the most stable point. In particular, the *intraSV* shows an average difference between the carotid and femoral angles of $6.22 \pm 3.14°$ in B1 compared with $14.87 \pm 7.15°$ in B2, indicating a smaller difference between the two waves at the two sites in the former case. Respectively for B1 and B2, Fig. 7(b) indicates for the carotid site (blue) a *interSV* of $73.10 \pm 3.14°$ and $43.04 \pm 9.84°$. At the femoral site (red), it is equal to $71.80 \pm 3.88°$ in the first point and $40.2 \pm 7.5°$ in the second. The average value is higher in B1 because, by definition, it represents the point of the maximal signal slope. In comparison, the standard deviation for the same location at the carotid and femoral sites is lower, indicating less variability in terms of slope among the 75 patients in the dataset. In view of the carried-out analysis, B1 proved to be the most stable point to be used for the application of the algorithm.

4.2. Pulse wave velocity assessment

Given the results reported in Table 3, it is possible to assume that the proposed algorithm is a viable option to provide a reliable assessment of cfPWV. The objective of the comparison was to assess our approach in relation to the technique utilized by the clinical gold standard used for non-invasive PWV assessment. The statistic indicators reported in the previous section determine the algorithm adopted by the Athos device (i.e., IT) as the best of the tested approaches. This result is attributable to the method adopted by the two devices. Both Athos and SphygmoCor use the intersecting tangent point as the algorithm for the estimation of PWV. In particular, Fig. 8(a) illustrates the outcomes of the linear regression model applied to the PWV values obtained from the Athos device in comparison to the Sphygmocor, exhibiting an R^2 value of 0.926. On the other hand, Fig. 8(b) depicts the concordance between the two methods in terms of mean value and average difference across the measurements. In this case, the Bland–Altman plot demonstrates an average difference, or bias, of −0.07 m/s for cfPWV values, along with narrow limits of agreement (LOA) values of 0.96 and −1.1. In contrast, the comparison between the direct application of cross-correlation (DCC) technique and SphygmoCor gave the worst results. The application of this approach, without the previously mentioned processing phases, was utilized to establish a starting point for evaluating the performance of the suggested method. In this case, the mean difference, the standard deviation, and the RMSE reached their highest values, -1.04 ± 2.21 m/s and 2.43 m/s respectively, while the

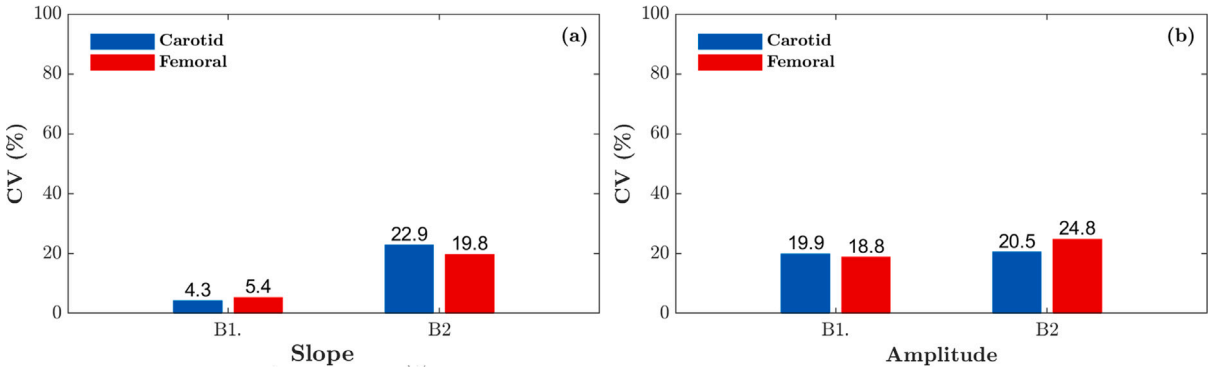

Fig. 6. Percentage coefficient of variation CV computed respectively in B1 and B2, on carotid (blue) and femoral (red) pulses. (**a**) CV extracted for the slope γ. (**b**) CV extracted for amplitude values.

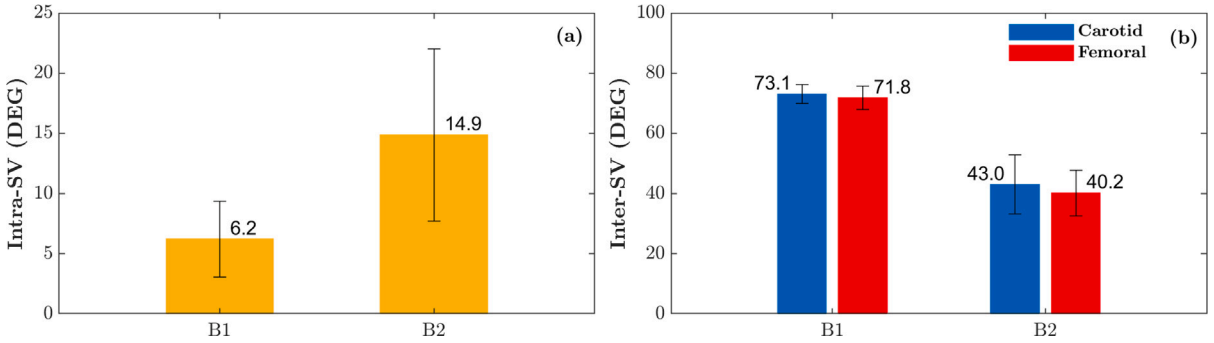

Fig. 7. (**a**) Intra-Subject Variability computed for γ respectively in B1 and B2. (**b**) Inter-Subject Variability computed for γ, respectively in B1 and B2, on carotid (blue) and femoral (red) pulses.

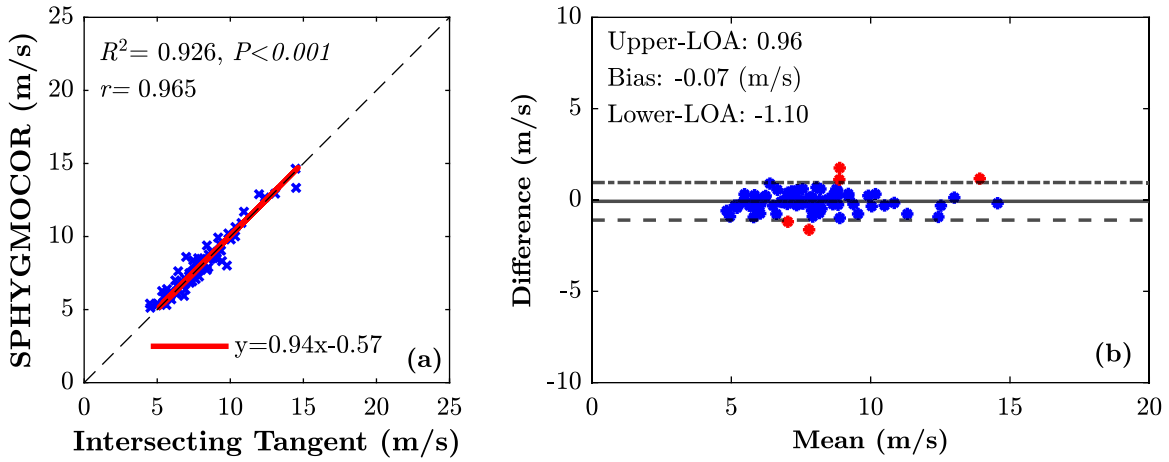

Fig. 8. Relationship between cfPWV estimated by the Intersecting Tangent algorithm used by the Athos device and the reference method. **(a)** Best fitted line (in red) retrieved from the linear regressive model fitted on the experimental data. **(b)** Bland–Altman plots show the distribution of the averaged measurements differences.

Pearson correlation coefficient and the coefficient of determination R^2 were equal to 0.82 and 0.638, Fig. 9(a). The reason for these results is the different morphology of the pulse wave when the proximal and distal sites are far apart confirming why this technique was applied just for a local evaluation of PWV. The lack of agreement of these two methods is also reflected in Fig. 9(b). Specifically, the systematic bias equal to −1.04 m/s along with a wider distribution of points and limits of agreement values respectively equal to 3.15 and −5.24 due to the presence of outliers in the PWV values. However, part of them was not included in Fig. 9(b) to keep the consistent scale on the y-axis along the three cases. The restriction of the comparison section combined with the normalization of the latter has made it possible to obtain a signal with a known shape while keeping the temporal information intact.

In line with the previous cases, Fig. 10 represents the linear regression model and the corresponding (Bland–Altman) plot. In this latter case, there is an improvement in all the presented statistical indicators. In particular, the bias is 0.16 while the R^2 and the r are respectively equal to 0.918 and 0.96. These values demonstrate a strong relationship between the predicted and observed values, indicating an excellent level of accuracy and agreement in the model's performance according to the performance criteria stated in the 2010 ARTERY Society guidelines [24] (mean difference < 0.5 m/s and SD < 0.8 m/s). From the comparison between the IT method and RBCC, it is possible to notice that the only substantial difference concerning the best case occurs for the average difference of the PWV values equal to −0.07 m/s and 0.16 m/s respectively. The RMSE in the two cases presents a difference

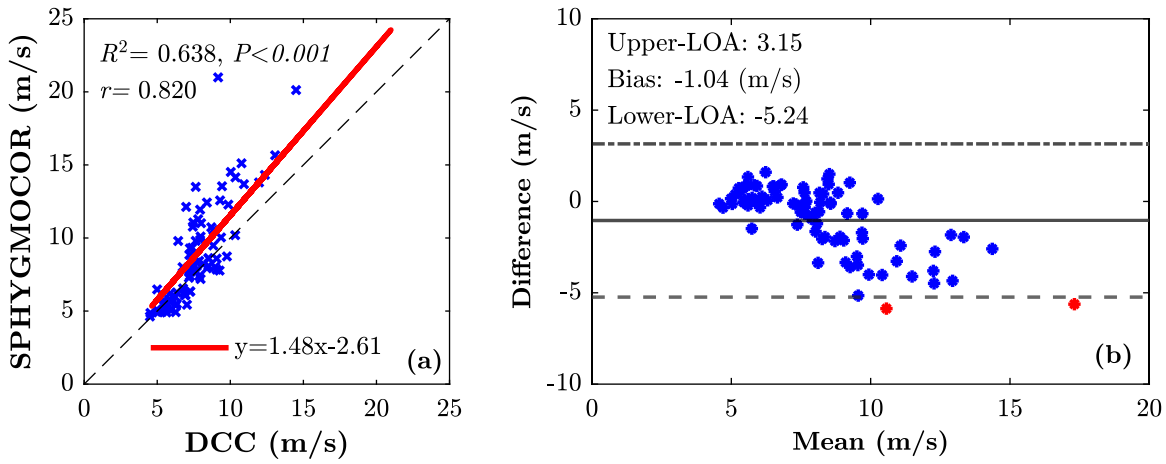

Fig. 9. Relationship between cfPWV estimated by the Direct application of Cross-Correlation (DCC) approach and the reference method. **(a)** Best fitted line (in red) retrieved from the linear regressive model fitted on the experimental data. **(b)** Bland–Altman plots show the distribution of the averaged measurements differences.

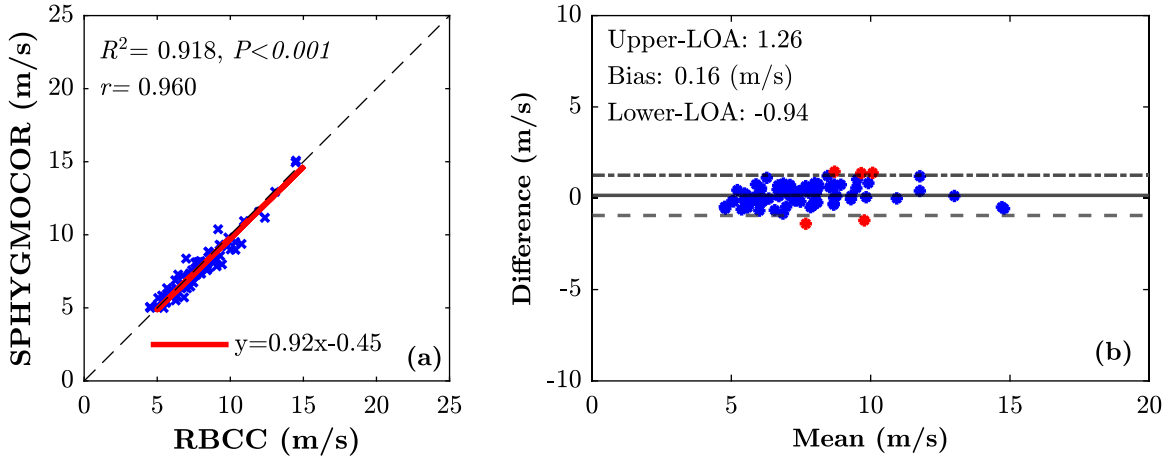

Fig. 10. Relationship between cfPWV estimated by the Region Based Cross-Correlation (RBCC) algorithm and the reference method. **(a)** Best fitted line (in red) retrieved from the linear regressive model fitted on the experimental data. **(b)** Bland–Altman plots show the distribution of the averaged measurements differences.

of less than 10%, while the standard deviation of the measurements mean difference, the Pearson correlation coefficient and the coefficient of determination R^2 present an average difference of less than 1%. The analysis conducted to determine the algorithm's robustness in the presence of different noise levels highlighted the greater tolerance of the latter compared to the IT method. Statistical significance was established using the Friedman test, which assessed the differences in cfPWV values between IT and RBCC across the four noise levels. In all tested cases, the P value consistently remained below 0.05, with three notably showing values largely below 0.01 (10^{-5}, 10^{-8}, and 10^{-8}, respectively, for 15, 20, and 25 dB). The exception occurred with an SNR of 10 dB where P resulted equal to 0.04. This outcome aligns with comparable values of mean absolute error and standard deviation reported in Fig. 5. In addition, it is necessary to consider that 10 dB represents a limiting case, which might not be suitable for a clinical application. Findings in [34] reveal an inverse relationship between RMSE and SNR at a constant sampling frequency, underscoring the substantial impact of SNR on estimation error. Furthermore, in [35], 15 dB was identified as the SNR value below which all the compared algorithms for peak detection showed a performance decline exceeding 20%. Finally, it is crucial to acknowledge that the acquisition process relies on a skilled operator who would reject a signal displaying distorted morphology. However, in all the remaining comparisons, the proposed method exhibited significantly reduced mean absolute error in the evaluation of the individual's PWV compared to the reference values derived from noise-free signals. This result highlights the impact of relying on a single feature in the signal for PTT assessment, indicating that errors in estimating PWV can be significant when detection is potentially affected by the presence of noise or artifacts. Furthermore, the assessment of PTT based on the realignment of pulse's upslope, and therefore for a higher number of data points, allows for mitigating a potential misdetection of points A or B in favor of a more robust and still accurate PWV assessment. Thus, although the RBCC method performs slightly differently from the intersecting tangent method, it turned out to be an excellent and more robust method to be used to estimate PWV. Furthermore, compared to the standard application of the cross-correlation approach, it was proved that through the reported processing steps it is possible to overcome the limitations responsible for the application of this technique to perform a local estimation of PWV. Our proposed approach's primary limitation stems from excluding non-healthy subjects during the validation process. This omission is noteworthy because non-healthy subjects are more likely to exhibit alterations in cfPWV associated with irregular vascular compliance and the potential impact of vasoactive medications. Regrettably, the ethical approval granted for this study imposes restrictions on testing the proposed algorithm exclusively on healthy subjects, as the use of the Athos device is authorized solely within the context of healthy individuals. In our future endeavors, we plan to extend the developed device's validation to include non-healthy subjects to validate the applicability and robustness of RBCC across a broader spectrum of health

conditions. A second limitation of our approach could be represented by the computational cost incurred by the cross-correlation process when comparing two windows on pulse waveforms to estimate cfPWV using a single feature. Nevertheless, it is crucial to note that the primary objective of this study is to explore the feasibility of the proposed algorithm for an offline assessment of cfPWV. The current focus is on the algorithm's performance in a non-real-time setting. Therefore, the optimization of the RBCC method for a real-time application will be further investigated in future works.

5. Conclusions

In this study, we presented a novel method for calculating cfPWV. The PTT is determined by computing the correlation between a specific portion of the signals, eliminating the requirement to identify characteristic points often utilized for this purpose. Particular attention was paid to finding an indicator that could be used to define the window on the signal. Thanks to the slope analysis, it was possible to locate the target section between the early systolic and end-diastolic portions of the blood pulses. Hence, by reducing the pulse wave section utilized for PWV assessment, we have developed an algorithm that yields results comparable to the gold standard employed in clinical practice. The proposed approach demonstrated that it is feasible to overcome the inherent limitation of the direct application of cross-correlation, which restricted its use in this sector to a local estimation. Moreover, for various SNRs, the RBCC algorithm was more robust than the IT method when applied to carotid and femoral pulse waveforms. Thus confirming the capability of the proposed approach to provide a non-invasive assessment of cfPWV in different conditions accurately and robustly. In conclusion, it was possible to prove that the RBCC algorithm is a suitable solution for assessing the cfPWV and it has the potential to be used in clinical practice as an alternative method to 'foot-to-foot' algorithms.

CRediT authorship contribution statement

Andrea Valerio: Writing – review & editing, Writing – original draft, Visualization, Validation, Software, Methodology, Investigation, Formal analysis, Data curation, Conceptualization. **Irene Buraioli:** Writing – review & editing, Writing – original draft, Visualization, Validation, Supervision, Software, Methodology, Investigation, Formal analysis, Data curation, Conceptualization. **Alessandro Sanginario:** Writing – review & editing, Writing – original draft, Visualization, Validation, Supervision, Methodology, Investigation, Formal analysis, Data curation, Conceptualization. **Giulia Mingrone:** Writing – review & editing, Visualization, Validation, Methodology, Investigation, Formal analysis, Data curation, Conceptualization. **Dario Leone:** Writing – review & editing, Visualization, Validation, Methodology, Investigation, Formal analysis, Data curation, Conceptualization. **Alberto Milan:** Writing – review & editing, Supervision, Software, Resources, Project administration, Methodology, Investigation, Funding acquisition, Conceptualization. **Danilo Demarchi:** Writing – review & editing, Supervision, Software, Resources, Project administration, Methodology, Investigation, Funding acquisition, Conceptualization.

Declaration of competing interest

The authors declare that they have no known competing financial interests or personal relationships that could have appeared to influence the work reported in this paper.

Data availability

Raw data is not currently available for sharing.

Acknowledgments

We would like to acknowledge and thank the participants, researchers, and clinicians for their contributions to this work. This research did not receive any specific grant from funding agencies in the public, commercial, or not-for-profit sectors.

References

[1] A. Laina, K. Stellos, K. Stamatelopoulos, Vascular ageing: Underlying mechanisms and clinical implications, Exp. Geront. 109 (2018) 16–30, http://dx.doi.org/10.1016/J.EXGER.2017.06.007, https://pubmed.ncbi.nlm.nih.gov/28624356.

[2] B.J. North, D.A. Sinclair, The intersection between aging and cardiovascular disease, Circ. Res. 110 (2012) 1097–1108, http://dx.doi.org/10.1161/CIRCRESAHA.111.246876, https://pubmed.ncbi.nlm.nih.gov/22499900.

[3] J. Blacher, A.P. Guerin, B. Pannier, S.J. Marchais, M.E. Safar, G.M. London, Impact of aortic stiffness on survival in end-stage renal disease, Circulation 99 (1999) 2434–2439, http://dx.doi.org/10.1161/01.CIR.99.18.2434, https://pubmed.ncbi.nlm.nih.gov/10318666.

[4] P.M. Nabeel, V.R. Kiran, J. Joseph, V.V. Abhidev, M. Sivaprakasam, Local pulse wave velocity: Theory, methods, advancements, and clinical applications, IEEE Rev. Biomed. Eng. 13 (2020) 74–112, http://dx.doi.org/10.1109/RBME.2019.2931587, https://pubmed.ncbi.nlm.nih.gov/31369386.

[5] W.W. Nichols, M.F. O'Rourke, E.R. Edelman, C. Vlachopoulos, Mcdonald's blood flow in arteries: theoretical, experimental and clinical principles: Seventh edition, McDonald's Blood Flow in Arteries: Theoretical, Experimental and Clinical Principles, seventh ed., 2022, pp. 1–821, http://dx.doi.org/10.1201/9781351253765.

[6] N. Westerhof, N. Stergiopulos, M.I. Noble, B.E. Westerhof, Snapshots of Hemodynamics: An Aid for Clinical Research and Graduate Education, 2018, pp. 1–314, http://dx.doi.org/10.1007/978-3-319-91932-4/COVER.

[7] C.K. Sun, Cardio-ankle vascular index (cavi) as an indicator of arterial stiffness, Integr. Blood Press. Control 6 (2013) 27–38, http://dx.doi.org/10.2147/IBPC.S34423, https://pubmed.ncbi.nlm.nih.gov/23667317.

[8] R. Mukkamala, J.O. Hahn, O.T. Inan, L.K. Mestha, C.S. Kim, H. Toreyin, S. Kyal, Toward ubiquitous blood pressure monitoring via pulse transit time: Theory and practice, IEEE Trans. Bio-Med. Eng. 62 (2015) 1879–1901, http://dx.doi.org/10.1109/TBME.2015.2441951, https://pubmed.ncbi.nlm.nih.gov/26057530.

[9] P. Boutouyrie, D. Fliser, D. Goldsmith, A. Covic, A. Wiecek, A. Ortiz, A. Martinez-Castelao, B. Lindholm, Z.A. Massy, G. Suleymanlar, R. Sicari, L. Gargani, G. Parati, F. Mallamaci, C. Zoccali, G.M. London, Assessment of arterial stiffness for clinical and epidemiological studies: methodological considerations for validation and entry into the european renal and cardiovascular medicine registry, nephrology, dialysis, Transplantation : Off. Publ. Eur. Dialysis Transpl. Assoc. Eur. Renal Assoc. 29 (2014) 232–239, http://dx.doi.org/10.1093/NDT/GFT309, https://pubmed.ncbi.nlm.nih.gov/24084326.

[10] P. Meani, A. Maloberti, P. Sormani, G. Colombo, L. Giupponi, M. Stucchi, M. Varrenti, P. Vallerio, R. Facchetti, G. Grassi, G. Mancia, C. Giannattasio, Determinants of carotid-femoral pulse wave velocity progression in hypertensive patients over a 3.7 years follow-up, Blood Pressure 27 (2018) 32–40, http://dx.doi.org/10.1080/08037051.2017.1378069, https://pubmed.ncbi.nlm.nih.gov/28922954.

[11] B.M. Pannier, A.P. Avolio, A. Hoeks, G. Mancia, K. Takazawa, Methods and devices for measuring arterial compliance in humans, Am. J. Hypertens. 15 (2002) 743–753, http://dx.doi.org/10.1016/S0895-7061(02)02962-X, https://pubmed.ncbi.nlm.nih.gov/12160200.

[12] M.A. Supiano, L. Lovato, W.T. Ambrosius, J. Bates, S. Beddhu, P. Drawz, J.P. Dwyer, N.M. Hamburg, D. Kitzman, J. Lash, E. Lustigova, C.M. Miracle, S. Oparil, D.S. Raj, D.E. Weiner, A. Taylor, J.A. Vita, R. Yunis, G.M. Chertow, M. Chonchol, Pulse wave velocity and central aortic pressure in systolic blood pressure intervention trial participants, PLoS One 13 (2018) http://dx.doi.org/10.1371/JOURNAL.PONE.0203305, https://pubmed.ncbi.nlm.nih.gov/30256784.

[13] I. Buraioli, D. Lena, A. Sanginario, D. Leone, G. Mingrone, A. Milan, D. Demarchi, A new noninvasive system for clinical pulse wave velocity assessment: The athos device, IEEE Trans. Biomed. Circuits Syst. 15 (2021) 133–142, http://dx.doi.org/10.1109/TBCAS.2021.3058010, https://pubmed.ncbi.nlm.nih.gov/33560991.

[14] B. Williams, G. Mancia, W. Spiering, E.A. Rosei, M. Azizi, M. Burnier, D.L. Clement, A. Coca, G.D. Simone, A. Dominiczak, T. Kahan, F. Mahfoud, J. Redon, L. Ruilope, A. Zanchetti, M. Kerins, S.E. Kjeldsen, R. Kreutz, S. Laurent, G.Y. Lip, R. McManus, K. Narkiewicz, F. Ruschitzka, R.E. Schmieder, E. Shlyakhto, C. Tsioufis, V. Aboyans, I. Desormais, G.D. Backer, A.M. Heagerty, S. Agewall, M. Bochud, C. Borghi, P. Boutouyrie, J. Brguljan, H. Bueno, E.G. Caiani, B. Carlberg, N. Chapman, R. Cífková, J.G. Cleland, J.P. Collet, I.M. Coman, P.W.D. Leeuw, V. Delgado, P. Dendale, H.C. Diener, M. Dorobantu, R. Fagard, C. Farsang, M. Ferrini, I.M. Graham, G. Grassi, H. Haller, F.D. Hobbs, B. Jelakovic, C. Jennings, H.A. Katus, A.A. Kroon, C. Leclercq, D. Lovic, E. Lurbe, A.J. Manolis, T.A. McDonagh, F. Messerli, M.L. Muiesan, U. Nixdorff, M.H. Olsen, G. Parati, J. Perk, M.F. Piepoli, J. Polonia, P. Ponikowski, D.J. Richter, S.F. Rimoldi,

M. Roffi, N. Sattar, P.M. Seferovic, I.A. Simpson, M. Sousa-Uva, A.V. Stanton, P.V.D. Borne, P. Vardas, M. Volpe, S. Wassmann, S. Windecker, J.L. Zamorano, Esc/esh guidelines for the management of arterial hypertension, Eur. Heart J. 39 (2018) (2018) 3021–3104, http://dx.doi.org/10.1093/EURHEARTJ/EHY339, https://pubmed.ncbi.nlm.nih.gov/30165516.

[15] L.M.V. Bortel, S. Laurent, P. Boutouyrie, P. Chowienczyk, J.K. Cruickshank, T.D. Backer, J. Filipovsky, S. Huybrechts, F.U. Mattace-Raso, A.D. Protogerou, G. Schillaci, P. Segers, S. Vermeersch, T. Weber, Expert consensus document on the measurement of aortic stiffness in daily practice using carotid-femoral pulse wave velocity, J. Hypertens. 30 (2012) 445–448, http://dx.doi.org/10.1097/HJH.0B013E32834FA8B0, https://pubmed.ncbi.nlm.nih.gov/22278144.

[16] F. Beutel, C.V. Hoof, X. Rottenberg, K. Reesink, E. Hermeling, Pulse arrival time segmentation into cardiac and vascular intervals - implications for pulse wave velocity and blood pressure estimation, IEEE Trans. Bio-Med. Eng. 68 (2021) 2810–2820, http://dx.doi.org/10.1109/TBME.2021.3055154, https://pubmed.ncbi.nlm.nih.gov/33513094.

[17] F.S. Hu, Y.L. Zhang, Z.C. Ma, Q.Q. Cao, Y.B. Xu, Z.J. He, Y.N. Sun, A region-matching method for pulse transit time estimation: potential for improving the accuracy in determining carotid femoral pulse wave velocity, J. Human Hypertens. 29 (2015) 675–682, http://dx.doi.org/10.1038/JHH.2015.9, https://pubmed.ncbi.nlm.nih.gov/25694218.

[18] H. Obeid, G. Soulat, E. Mousseaux, S. Laurent, N. Stergiopulos, P. Boutouyrie, P. Segers, Numerical assessment and comparison of pulse wave velocity methods aiming at measuring aortic stiffness, Physiol. Meas. 38 (2017) 1953–1967, http://dx.doi.org/10.1088/1361-6579/AA905A, https://pubmed.ncbi.nlm.nih.gov/28968226.

[19] O. Vardoulis, T.G. Papaioannou, N. Stergiopulos, Validation of a novel and existing algorithms for the estimation of pulse transit time: advancing the accuracy in pulse wave velocity measurement, Am. J. Physiol. Heart Circ. Physiol. 304 (2013) http://dx.doi.org/10.1152/AJPHEART.00963.2012, https://pubmed.ncbi.nlm.nih.gov/23604712.

[20] Y.C. Chiu, P.W. Arand, S.G. Shroff, T. Feldman, J.D. Carroll, Determination of pulse wave velocities with computerized algorithms, Am. Heart J. 121 (1991) 1460–1470, http://dx.doi.org/10.1016/0002-8703(91)90153-9, https://pubmed.ncbi.nlm.nih.gov/2017978.

[21] S.C. Millasseau, A.D. Stewart, S.J. Patel, S.R. Redwood, P.J. Chowienczyk, Evaluation of carotid-femoral pulse wave velocity: influence of timing algorithm and heart rate, Hypertension (Dallas, Tex. : 1979) 45 (2005) 222–226, http://dx.doi.org/10.1161/01.HYP.0000154229.97341.D2, https://pubmed.ncbi.nlm.nih.gov/15642772.

[22] P. Salvi, E. Magnani, F. Valbusa, D. Agnoletti, C. Alecu, L. Joly, A. Benetos, Comparative study of methodologies for pulse wave velocity estimation, J. Human Hypertens. 22 (2008) 669–677, http://dx.doi.org/10.1038/JHH.2008.42, https://pubmed.ncbi.nlm.nih.gov/18528411.

[23] S. Seoni, S. Beeckman, Y. Li, S. Aasmul, U. Morbiducci, R. Baets, P. Boutouyrie, F. Molinari, N. Madhu, P. Segers, Template matching and matrix profile for signal quality assessment of carotid and femoral laser doppler vibrometer signals, Front. Physiol. 12 (2022) http://dx.doi.org/10.3389/fphys.2021.775052.

[24] I.B. Wilkinson, C.M. McEniery, G. Schillaci, P. Boutouyrie, P. Segers, A. Donald, P.J. Chowienczyk, Artery society guidelines for validation of non-invasive haemodynamic measurement devices: Part 1, arterial pulse wave velocity, Artery Res. 4 (2010) 34–40, http://dx.doi.org/10.1016/J.ARTRES.2010.03.001.

[25] L. Xu, S. Zhou, L. Wang, Y. Yao, L. Hao, L. Qi, Y. Yao, H. Han, R. Mukkamala, S.E. Greenwald, Improving the accuracy and robustness of carotid-femoral pulse wave velocity measurement using a simplified tube-load model, Sci. Rep. 12 (2022) http://dx.doi.org/10.1038/S41598-022-09256-Z, https://pubmed.ncbi.nlm.nih.gov/35338246.

[26] H. Shin, A. Choi, Calculation and validation of continuous pulse transit time based on normalized pulse wave velocity, IEEE Access 8 (2020) 221632–221639, http://dx.doi.org/10.1109/ACCESS.2020.3041498.

[27] D. Leone, I. Buraioli, G. Mingrone, D. Lena, A. Sanginario, F. Vallelonga, F. Tosello, E. Avenatti, M. Cesareo, A. Astarita, L. Airale, L. Sabia, F. Veglio, D. Demarchi, A. Milan, Accuracy of a new instrument for noninvasive evaluation of pulse wave velocity: the arterial stiffness faithful tool assessment project, J. Hypertens. 39 (2021) 2164–2172, http://dx.doi.org/10.1097/HJH.0000000000002925.

[28] A.L. Wentland, T.M. Grist, O. Wieben, Review of mri-based measurements of pulse wave velocity: A biomarker of arterial stiffness, Cardiovasc. Diagn. Therapy 4 (2) (2014) 193–206.

[29] P. Charlton, J. Mariscal Harana, S. Vennin, Y. Li, P. Chowienczyk, A. J, Modeling arterial pulse waves in healthy aging: a database for in silico evaluation of hemodynamics and pulse wave indexes, Am. J. Physiol. Heart. Circ. Physiol. 82 (1) (2019) 1062–1065.

[30] J.A. Chirinos, N. Sweitzer, Ventricular–arterial coupling in chronic heart failure, Cardiac Fail. Rev. 03 (2017) 12, http://dx.doi.org/10.15420/cfr.2017:4:2, https://www.cfrjournal.com/articles/ventricular-arterial-coupling-chronic-heart-failure.

[31] Y. Chiu, P.W. Arand, S.G. Shroff, T. Feldman, J.D. Carroll, Determination of pulse wave velocities with computerized algorithms, Am. Heart J. 121 (5) (1991) 1460–1470, https://www.sciencedirect.com/science/article/pii/0002870391901539.

[32] S. Laurent, J. Cockcroft, L. Van Bortel, P. Boutouyrie, C. Giannattasio, D. Hayoz, B. Pannier, C. Vlachopoulos, I. Wilkinson, H. Struijker-Boudier, Expert consensus document on arterial stiffness: Methodological issues and clinical applications, Eur. Heart J. 27 (21) (2006) 2588–2605, http://dx.doi.org/10.1093/eurheartj/ehl254, cited by: 4759; All Open Access, Bronze Open Access.

[33] C. Argyriou, E. Georgakarakos, G.S. Georgiadis, N. Schoretsanitis, M.K. Lazarides, The effect of revascularization on the hemodynamic profile of patients with infrarenal aortic occlusion, Annals Vasc. Surg. 43 (2017) 210–217, http://dx.doi.org/10.1016/j.avsg.2016.11.025.

[34] S. Zaunseder, A. Vehkaoja, V. Fleischhauer, C.H. Antink, Signal-to-noise ratio is more important than sampling rate in beat-to-beat interval estimation from optical sensors, Biomed. Signal Process. Control 74 (2022) 103538, http://dx.doi.org/10.1016/j.bspc.2022.103538.

[35] K. Kazemi, J. Laitala, I. Azimi, P. Liljeberg, A.M. Rahmani, Robust ppg peak detection using dilated convolutional neural networks, Sensors 22 (2022) 6054, http://dx.doi.org/10.3390/s22166054.